HHS Public Access

Author manuscript

J Biophotonics. Author manuscript; available in PMC 2020 March 01.

Published in final edited form as:

J Biophotonics. 2019 March ; 12(3): e201800205. doi:10.1002/jbio.201800205.

Super-achromatic Optical Coherence Tomography Capsule for Ultrahigh-resolution Imaging of Esophagus

Kaiyan Li[†], **Wenxuan Liang**[2], **Jessica Mavadia-Shukla**[2], **Hyeon-Cheol Park**[2], **Dawei Li**[2], **Wu Yuan**[2], **Suiren Wan**[1], and **Xingde Li**[2,*]

[1]School of Biological Science & Medical Engineering, Southeast University, Nanjing, Jiangsu, China 210096

[2]Department of Biomedical Engineering, Johns Hopkins University, Baltimore, MD, USA 21205

Abstract

Endoscopic optical coherence tomography (OCT) is a noninvasive technology allowing for imaging of tissue microanatomies of luminal organs in real time. Conventional endoscopic OCT operates at 1,300 nm wavelength region with a sub-optimal axial resolution limited to 8–20 μm. In this paper we present the first ultrahigh-resolution tethered OCT capsule operating at 800 nm and offering about 3–4 fold improvement of axial resolution (plus enhanced imaging contrast). The capsule uses diffractive optics to manage chromatic aberration over a full ~200 nm spectral bandwidth centering around 830 nm, enabling to achieve super-achromaticity and an axial resolution of ~2.6 μm in air. The performance of the OCT capsule is demonstrated by volumetric imaging of swine esophagus *ex vivo* and sheep esophagus *in vivo*, where fine anatomic structures including the sub-epithelial layers are clearly identified. The ultrahigh resolution and excellent imaging contrast at 800 nm of the tethered capsule suggest the potential of the technology as an enabling tool for surveillance of early esophageal diseases on awake patients without the need for sedation.

Graphic Abstract

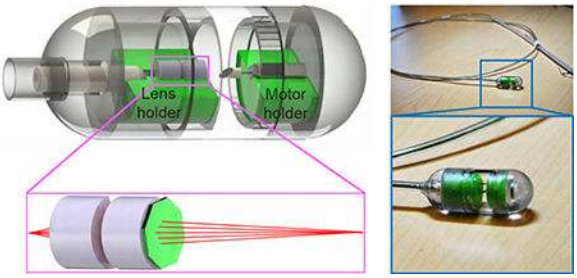

Keywords

endoscopic optical coherence tomography; capsule; ultrahigh resolution; super-achromatic; esophagus

[*]Corresponding author. xingde@jhu.edu.
[†]This work was done while the author was at JHU

1. Introduction

Barrett's esophagus (BE) is a gastrointestinal complication where squamous epithelium is damaged by chronic gastroesophageal reflux and replaced by metaplastic columnar epithelium [1]. As an incomplete form of intestinal metaplasia, BE predisposes patients to esophageal adenocarcinoma (EA) [2], a lethal condition with only a 10–15% five-year survival rate [3], and its incidence has increased by more than 7-fold over the past decades [4], presenting significant economic and societal burdens. Periodic screening is crucial for early EA detection, so that timely intervention (such as mucosal resection) can be undertaken to prevent EA from progressing into more lethal stages. Previous clinical studies have demonstrated that for BE patients who are diagnosed with EA, approximately 86% of EA cases were detected at earlier stages by performing periodic surveillance, leading to a high 2-year survival rate of about 43.3% [5]. Therefore, rigorous periodic upper endoscopy is adopted as a clinical standard of care for BE patients [6, 7].

The current gold standard for definitive esophageal cancer diagnosis is endoscopic guided biopsy followed by histopathology inspection [8], which is time-consuming. To minimize the chance of missing inconspicuous lesions that might spread over BE, the current protocol recommends four-quadrant biopsies every ≤ 2 cm along the full length of BE. While inflicting substantial trauma to the patients, such a dense sampling strategy is still prone to sampling errors and misdiagnosis [9, 10]. In addition to the limited biopsy areas compared with the entire esophagus surface, one central reason for inefficient biopsy is that conventional clinical optical endoscopy can only visualize the superficial esophageal mucosa with a macroscopic resolution and cannot probe deep into the mucosa to interrogate morphology changes of tissues underneath the mucosa surface. An ideal solution would be a non-invasive, depth-resolved endoscopic microscopy modality with histology-level resolution over the entire esophagus so that suspicious lesions could be identified *in vivo* and in real time.

One promising modality is optical coherence tomography (OCT) [11, 12], an intrinsically depth-resolved imaging technology capable of cross-sectional visualization of tissue micro structures 0.5–2.5 mm below the tissue surface. High-speed three-dimensional OCT imaging of the entire esophagus could be completed within only a few minutes. Pilot *ex vivo* studies have suggested that OCT holds a strong promise for detecting epithelial morphological changes in BE [13–15]. To enable *in vivo* imaging, small-diameter (e.g., ~2 mm), fiber-optic OCT catheters deliverable through the accessory port of standard upper gastrointestinal endoscopes have been developed for intraluminal surveillance of the esophagus [16]; however, it is challenging to stabilize such a thin catheter in the center of a large lumen as the esophagus. A better solution is OCT balloon catheters which, after passing the accessory port, can be inflated to expand until fully contacting the mucosa surface of the esophagus [16–18]. One shortcoming of using a balloon catheter is that OCT imaging needs to be conducted via a traditional endoscope, and therefore requires patient sedation, a specialized endoscopy suite and professionals, which are labor-intensive, time-consuming, and costly [5]. Furthermore, the longitudinal scanning range of a balloon catheter, once inflated, is restricted to the portion of esophagus that is in contact with the balloon [19]. To address

these limitations and to scan quickly through the entire esophagus, a tethered endoscopic OCT capsule has become an attractive alternative [20, 21]. By capitalizing on patients' inherent swallowing and esophageal peristalsis ability, such a capsule-shaped endoscope eliminates the need for sedation, and thus can perform imaging more effectively both in cost and time.

Tethered OCT capsules reported so far operate at 1,300 nm with an excellent axial resolution of ~7.0–8.5 μm and lateral resolution of ~26–30 μm (in tissue) [20, 21]. It is desirable to have a better resolution in order to better identify fine morphological changes associated with EA. Given the quadratic dependence of axial resolution on the center wavelength of the light source, moving the central wavelength from 1,300 nm to 800 nm can significantly promote axial resolution, as first demonstrated in a bench-top system which achieves an axial resolution of ~1.5 μm (in air) [22] and later in endoscopic systems with axial resolution of 2.2~3.2 μm in air [23–27]. However, to the best of our knowledge, these reported 800 nm endoscopes all featured a short focal length (< 1.5 mm). For a singlet lens, according to the relationship between the ratio of focal length to chromatic longitudinal focal shift and the Abbe number ($-\frac{f}{df} = v$) [28], a longer focal length gives rise to larger axial color aberration. For an imaging capsule, the required long focal length (~10 mm) exacerbates the chromatic aberration and thereby more severely deteriorates the axial resolution.

In this paper we present the first ultrahigh-resolution tethered OCT imaging capsule. By correcting the severe chromatic aberration using a cost effective customized diffractive lens, an axial resolution of ~2.6 μm in air was achieved, which corresponds to ~1.84 μm in tissue assuming a tissue refractive index of 1.4. The capsule can perform video-rate (20 frames/s) OCT imaging via distal-end micromotor-based circumferential scanning with negligible non-uniform rotational distortion. Results of real-time imaging of swine esophagus *ex vivo* and sheep esophagus *in vivo* demonstrated the ultrahigh resolution, high contrast and large field of view afforded by this newly-developed OCT endoscopic capsule, suggesting its potential as an effective screening technology for pathological changes in the esophagus.

2. Materials and Methods

2.1. System setup

The details of our home-built ultrahigh-resolution spectral-domain OCT system was described in our previous report [25]. In essence, it consists of a home-built broadband Ti:Sapphire laser, a customized broadband fiber-optic Michelson interferometer, and a custom-designed broadband linear-k OCT imaging spectrometer. The laser has a central wavelength of ~830 nm and a 3dB spectral bandwidth of ~150 nm. The customized imaging spectrometer consists of 2,048 pixels and can accommodate 250 nm in spectral bandwidth with a maximum data acquisition speed of 70k A-lines per second at a 12-bit digitization resolution. Limited by the A-line scan rate of CCD used in the spectrometer, the ultimate imaging speed was 20 frames/s with each frame consisted of 3500 A-lines.

2.2. *Ex vivo* animal preparation and image acquisition

All animal housing and experimentation procedures were performed in accordance with the standards of humane animal care described in the National Institutes of Health Guide for the Care and Use of Laboratory Animals, with protocols approved by the institutional animal care and use committee of the Johns Hopkins University. Immediately after the swine was sacrificed (60 pounds, Archer Farm) the fresh esophagus was harvested and then pinned to a wax block. The capsule was gently inserted and positioned in the distal end of the esophagus. 3D volumetric imaging was performed by the longitudinal pullback of the capsule while the beam was scanned circumferentially by the micromotor. The imaged segment of the esophagus was harvested for histologic processing.

2.3. *In vivo* animal preparation and image acquisition

The sheep (40 pounds, Archer farm) was fasted the day prior to the experiment. Anesthesia was initiated with intramuscular ketamine (25 mg/kg) and subsequently maintained with intravenous propofol given into a jugular vein (0.8 mg/kg/min). The sheep was then ventilated with fresh room air with a volume of 15 ml/kg at a rate of 15/min. Depth of anesthesia was monitored by lash reflex, heart rate (via EKG), and respiration. Ventilation pressure and end tidal CO_2 were measured and recorded and were used to assess the adequacy of ventilation. With the sheep anesthetized, the capsule was directly inserted into its esophagus under the guidance of real time OCT imaging until the capsule reached the gastro-esophageal junction. B-scan images were collected by pulling back the capsule tether by a linear translation stage or insertion by hand. After OCT imaging, the sheep was sacrificed and the esophagus was harvested and fixed in formalin immediately followed by standard histology processing.

2.4. Endoscopic OCT laser ablation marking setup

Laser ablation marking was performed using a conventional home-built OCT imaging catheter made of a single-mode fiber for 1,300 nm (SMF28), a spacer, a GRIN lens and a reflector [16, 18]. All the components were designed and tested for transmitting at least 500 mW of laser power at 1470 nm for tissue ablation. After imaging the normal tissues, the OCT capsule was retracted and the ablation catheter was introduced into the esophagus. The inserting depth of the ablation catheter was recorded to facilitate positioning the imaging capsule to the ablation region for tissue harvesting. A shutter with a timer was used to control the exposure time of the ablation laser.

3. Results and Discussion

3.1. Distal scanning OCT imaging capsule

Illustrated in Fig. 1A is the design schematic of the tethered OCT imaging capsule. It comprises an 8-degree angle cleaved single-mode fiber (SMF), two achromatic lenses along with a diffractive lens (Fig. 1B), a microreflector, and a micromotor. The distal end of the SMF was fixed within a ferrule, delivering illumination light to the capsule. The achromatic diffractive optics focused the imaging beam approximately 8 mm away from the diffractive lens to provide a sufficient working distance needed for large lumen imaging. The

microreflector was mounted on the micromotor shaft and deflected the beam by ~100 degrees for side viewing imaging. Outside the capsule, the SMF was enclosed inside a flexible torque coil; the torque coil and the micromotor drive wires were encased within a biocompatible grade plastic tube. In parallel with electrical wires of the micromotor, the torque coil was in turn housed inside a tubular plastic sheath. Ideally, for human study, the torque coil and plastic sheath should be as thin and pliable as possible to ease swallowing; for imaging studies on anesthetized animal models, however, a more rigid plastic sheath was purposely selected to facilitate the insertion of the capsule into the animal's esophagus. 3D imaging was achieved by pulling back or advancing the capsule through the tether (torque and plastic sheath), while circumferentially scanning the imaging beam by rotating the reflector with a 2.4 mm-diameter micromotor situated within the capsule (Fig. 1A). Compared with proximal beam scanning, the micromotor-based distal beam scanning minimizes non-uniform rotational distortion (NURD), caused by the fiber bending, twisting and rotational friction and the associated imaging artifacts [29, 30]; however, it is sometimes accompanied with another form of NURD induced by the mechanical instability of the micromotor [31, 32]. After each experiment, the capsule was retrieved for reuse after going through a standard endoscope disinfection procedure [33]. Fig. 1D shows a photograph of a 2-meter-long tethered endoscopic OCT capsule with a close-up view of the capsule shown in Fig. 1D, which has a size 13 mm × 30 mm (diameter × length).

The achromat and diffractive lenses are the key components for correcting chromatic aberration and achieving high axial resolution. It is well known that chromatic aberration induced by material dispersion is more pronounced around 800 nm than 1,300 nm. Commonly described by longitudinal focal shift, chromatic aberration can severely degrade axial resolution and thus image quality. For our OCT capsule, such intrinsic aberration is challenging to handle when considering the broad overall 200 nm-wide source spectral bandwidth and the long focal length (~ 10 mm). To overcome this challenge, we first carefully selected two achromatic doublets (Edmund 84127 and Thorlabs AC05010B) to correct the majority of the chromatic aberration. Nevertheless, according to ray-tracing simulations (Fig. 2A, blue curve), the combination of the two doublets still resulted in a longitudinal focal shift of ~110 μm over the 750–950 nm spectral range, which was much larger than the theoretical axial resolution (~2–3 μm) afforded by the broadband light source. As we previously demonstrated in detail [25], such a large uncorrected longitudinal focal shift severely degraded the axial resolution.

To further suppress the focal shift, a customized diffractive lens (DL) for a specific spectrum range from 750 – 950 nm with a NA of 0.05 was attached directly to the focusing lens (the one before the reflector) by optical adhesive. The DL has several concentric rings etched on a micro-lens as shown in Fig. 1B, and the design details can also be found in Reference [27] recently published by our group. As shown by the red curve in Fig. 2A, the longitudinal focal shift was dramatically reduced to ~2 μm over the full 200 nm bandwidth. To experimentally verify the achromaticity of the capsule, we measured the back-reflected spectra by placing a mirror at the focal plane of the compound imaging optics, and then translating it along the imaging depth by 500 μm. As shown in Fig. 2B, the back-reflected spectra remained nearly unchanged at different imaging depths. A measured representative

axial point spread function is shown in Fig. 2C, revealing an FWHM of ~2.6 μm (i.e., the axial resolution in air). The lateral resolution is ~15 μm in air, and the final working distance was measured to be ~300 μm outside of the 13-mm-diameter capsule shell.

The capsule body comprises three parts: the proximal cap, the cylindrical shell and the distal cap. The cylindrical shell was further built from three segments of transparent tubes glued together. The two segments joined with the proximal and distal caps are made of 1.6-mm thick plastic, while the middle one is made of a 1-mm thick glass shell in order to increase transmission and minimize astigmatism (ASTI). To facilitate the assembling process, self-aligned plastic holders (green components in Fig. 1A) were specially designed and fabricated via high-resolution 3D printing, which support the fiber (inside a ferrule), the lenses and the micromotor, and keep them concentric with respect to the glass shell of the capsule.

ASTI, arising from the cylindrical shell, diverges beam along the azimuthal direction, and degenerates lateral resolution. The dependence of ASTI on the shell radius and thickness has been discussed [18]. Given the glass shell thickness of 1 mm, we investigated the focal spot shape and the ASTI over the DOF by ray-tracing simulations, and the result is illustrated in Fig. 3A. The worst case was indicated by the red dashed box, where the geometric spot remains much smaller than the Airy disk meaning the resulted spot shape is totally acceptable. This was also verified by experimental results: the measured worst spot shape (Fig. 3B) over the DOF has a ratio of the long to short axis approximately 1.6, which was slightly distorted from the optimal one with a measured ratio of about 1 at the focal plane (Fig. 3C).

3.2 *Ex vivo* swine esophagus imaging

Ex vivo swine esophagus imaging was performed by using a home-built ultrahigh-resolution spectral-domain OCT (see Methods) with an excellent axial resolution of ~2.6 μm to demonstrate the imaging performance of the capsule. After the deployment of the capsule into the esophagus, circumferential scanning was performed by the micromotor together with longitudinal pullback for 3D volumetric imaging. Figure 4 illustrates some representative *ex vivo* OCT images of swine esophagus acquired by the 800 nm OCT capsule. Shown in Fig. 4A is an unwrapped rectangular cross-sectional image of the esophagus. To better appreciate the fine layer structures revealed by the capsule, a close-up of one portion (red dashed box) of the image is shown in Fig. 4B, which clearly shows five distinct layers of a normal swine esophagus extending from the stratified squamous epithelium to lamina propria, muscularis mucosae, submucosa and muscularis propria. Structures shown in Fig. 4B correlate qualitatively with a representative histology shown in Fig. 4C. The superb resolution and high contrast of the 800 nm capsule allow us to recognize more fine features which are not generally visible with a conventional 1,300 nm OCT system. First, sublayers within EP (line arrows in Fig. 4B and Fig. 4C) were identified: in Fig. 4B, scattering of EP is mild in the top sublayer, strong in the middle sublayer and weak in the bottom sublayer, which roughly correspond to mature EP, embryonic EP and basal EP sublayers, respectively. Second, the adipose and glands (blue arrows in Fig. 4B and Fig. 4C) in the SM layer were very pronounced. Neither the EP sublayers nor the adipose and glands

could be distinguished such clearly in images acquired by conventional 1,300 nm endoscopes which had a resolution of 8.6 μm × 28.0 μm (axial × lateral, in tissue) [16]. Compared with OCT capsules working at 1,300nm with a resolution of ~7.0–8.5 μm × 26–30 μm (axial × lateral, in tissue) [21, 22], glands and adipose tissues were much clearer and the layer boundaries were much sharper in the images collected by the 800 nm capsule from normal tissue samples. By pulling the capsule over an ~20 mm distance with 20 μm pitch, a 3D volumetric image of the lower esophagus was acquired and rendered as shown in Fig. 4D. The layered structures described above are also manifest in the 3D image. The front cross-section pointed by green arrow in Fig. 4D is displayed in Fig. 4E. It is also worth noting that, no obvious NURD-induced distortion was noticed in this data set displayed here.

3.3. *In vivo* sheep esophagus imaging and laser marking

To further assess the imaging performance of the capsule in terms of ultrahigh resolution and enhanced contrast, and to verify its capability of imaging various animal models, *in vivo* sheep esophagus imaging was also conducted (see Methods). Fig. 5A illustrates a representative cross-sectional image of the sheep esophagus *in vivo*. A couple of non-contact areas were noticed on the image as indicated by the brackets, which resulted from esophageal expansion during peristalsis. Fig. 5B is a close-up of the red dashed box indicated in Fig. 5A. Comparing to its corresponding histology (Fig. 5C), the boundaries between the LP and MM, MM and SM, and between the three sublayers in EP are distinct. Comparing to *ex vivo* swine images (Fig. 4), *in vivo* sheep images have much higher contrast and sharper boundaries. Another obvious difference is that the EP layer in sheep (as ruminant) is thicker than that in swine if comparing Fig. 4B to Fig. 5B, or Fig. 4C to Fig. 5C.

As a very promising tool for guiding tissue biopsy during endoscopy, tissue marking by laser ablation has been demonstrated in a 1300 nm endoscopic OCT system [34]. In this paper, we examine the power and duration needed to create visible landmarks for preparing future integration of laser ablation with the 800 nm OCT endoscopic capsule in a seamless fashion. By using a conventional home-built OCT imaging catheter (see Methods), tissue was coagulated and the color of tissue turned white within 5s (see the left white spot in Fig. 5E) with an approximately 150 mW incident power on the tissue surface, while with an ~300 mW power, tissue denatured in a second (see the right white spot in Fig. 5E), and was more visible than the left one. Shown in Fig. 5D is a representative *in vivo* cross-sectional image of sheep esophagus following laser ablation. Ablation marks featuring abnormally darkened regions in the superficial layer with outer layers becoming invisible (indicated by red arrowheads in Fig. 5D) can be easily identified.

3.4 Discussion

A tethered OCT endoscopic capsule operating at 800 nm was successfully developed. Its excellent imaging resolution and contrast were demonstrated on real-time, large circumference and volumetric OCT imaging of swine *ex vivo* and sheep esophagus *in vivo*. The capsule employs customized diffractive optics and a thin glass shell to minimize chromatic aberration and astigmatism. Its excellent imaging performance and capability of imaging a large tissue area are manifest in three aspects. Firstly, the ~2.6 um axial resolution

and excellent imaging contrast at 800 nm enable identification of all 5 layers of the esophagus as well as other fine tissue microstructures such as glands and adipose. Secondly, the capability of discerning the three sublayers in the EP suggests the potential of the ultrahigh-resolution imaging capsule for differentiating earlier pathological changes in the esophagus (including dysplasia), which are often associated with basal epithelium cells enlargement and crowding [35]. Thirdly, boundaries between LP and MM and between MM and SM layers in OCT images were as evident and well-defined as in histology micrographs, suggesting the possibility of using the ultrahigh-resolution 800 nm OCT capsule for detecting lesions that invade across the LP/MM and MM/SM boundaries.

NURD is not uncommon in micromotor-based OCT endoscopes [31, 32]. In our capsule NURD occurred from time to time and usually accounted for 5%−10% of the total A-line number when it happened. Light load, sufficient driving voltage and rotation speed for the micromotor can improve the micromotor performance and reduce NURD [36]. Several methods have been developed for effectively removing the NURD [31, 32, 37, 38].

In this study, the laser ablation catheter was used independently from the imaging capsule. In the future, the laser marking function will be integrated into the OCT capsule in order to be a practical guiding tool for tissue biopsy during the same endoscopic procedure as imaging. Moreover, OCT capsule based laser ablation might also serve as a BE treatment method with a carefully controlled laser power and exposure time [39] while monitoring tissue coagulation in real time.

A potential limitation in shifting the central wavelength from 1,300 nm to 800 nm is the imaging depth. Nevertheless, based on OCT images shown in Fig. 4 and Fig. 5, though part of muscularis external, myenteric plexus and adventitia are missing, the four representative layers (EP, LP, MM, and SM) plus a portion of the fifth layer – MP were clearly identified in esophagus with an imaging depth of about 700 μm. For human esophagus, this imaging depth might be sub-optimal, but it is comparable with the biopsy depth for detecting earlier lesions.

Price is an important and practical concern in clinic translation. Ti:Sapphire laser was used in our current study for convenient proof of concept tests on an existing bench-top SD-OCT setup. A portable super-continuum light source is an economical alternative, and its effectiveness in OCT imaging in the 800 nm wavelength range has been demonstrated in our previous work [26]. In terms of the lenses including the customized diffractive lens, they are not very expensive with the total cost less than $300, and the price can drop dramatically in mass production.

Acknowledgements

This research was supported partially by the National Institutes of Health under grants R01CA153023 and R01HL121788 (X.D.L.) and China Scholarship Council (K.Y. L.). The authors gratefully thank Robert Brown, Jeffery Loube, Laurie Pipitone and Juls A. Meyers for helpful discussions and assistance with *in vivo* experiments, and Honghua Guan for help with components machining.

References

[1]. Spechler SJ, N Engl J Med. 2002, 346, 836. [PubMed: 11893796]

[2]. Reid BJ, Li X, Galipeau PC, Vaughan TL, Nat Rev Cancer. 2010, 10, 87. [PubMed: 20094044]

[3]. Shaheen NJ, Richter JE, Lancet. 2009, 373, 850. [PubMed: 19269522]

[4]. Spechler SJ, JAMA. 2013, 310, 627. [PubMed: 23942681]

[5]. Sharma P, Sidorenko EI, Gut. 2005, 54 Suppl 1, i27. [PubMed: 15711005]

[6]. Wang KK, Sampliner RE, Practice G Parameters Committee of the American College of, Am J Gastroenterol. 2008, 103, 788. [PubMed: 18341497]

[7]. Zakko L, Lutzke L, Wang KK, Minerva Med. 2017, 108, 28. [PubMed: 27792223]

[8]. Repaka A, Chak A, Nat Rev Gastroenterol Hepatol 2011, 8, 582. [PubMed: 21894201]

[9]. Levine DS, Haggitt RC, Blount PL, Rabinovitch PS, Rusch VW, Reid BJ, Gastroenterology. 1993, 105, 40. [PubMed: 8514061]

[10]. Spechler SJ, Am J Gastroenterol. 2005, 100, 927. [PubMed: 15784042]

[11]. Huang D, Swanson EA, Lin CP, Schuman JS, Stinson WG, Chang W, Hee MR, Flotte T, Gregory K, Puliafito CA, et al., Science. 1991, 254, 1178. [PubMed: 1957169]

[12]. Fujimoto JG, Pitris C, Boppart SA, Brezinski ME, Neoplasia. 2000, 2, 9. [PubMed: 10933065]

[13]. Bouma BE, Tearney GJ, Compton CC, Nishioka NS, Gastrointest Endosc. 2000, 51, 467. [PubMed: 10744824]

[14]. Sivak MV, Kobayashi K, Izatt JA, Rollins AM, Ung-runyawee R, Chak A, Wong RCK, Isenberg GA, Willis J, Gastrointest Endosc. 2000, 51, 474. [PubMed: 10744825]

[15]. Li XD, Boppart SA, Van Dam J, Mashimo H, Mutinga M, Drexler W, Klein M, Pitris C, Krinsky ML, Brezinski ME, Fujimoto JG, Endoscopy. 2000, 32, 921. [PubMed: 11147939]

[16]. Fu HL, Leng Y, Cobb MJ, Hsu K, Hwang JH, Li XD, J Biomed Opt. 2008, 13, 060502. [PubMed: 19123643]

[17]. Suter MJ, Vakoc BJ, Yachimski PS, Shishkov M, Lauwers GY, Mino-Kenudson M, Bouma BE, Nishioka NS, Tearney GJ, Gastrointest Endosc. 2008, 68, 745. [PubMed: 18926183]

[18]. Xi JF, Huo L, Wu Y, Cobb MJ, Hwang JH, Li XD, Opt Lett. 2009, 34, 1943. [PubMed: 19571960]

[19]. Vakoc BJ, Shishko M, Yun SH, Oh WY, Suter MJ, Desjardins AE, Evans JA, Nishioka NS, Tearney GJ, Bouma BE, Gastrointest Endosc. 2007, 65, 898. [PubMed: 17383652]

[20]. Gora MJ, Sauk JS, Carruth RW, Gallagher KA, Suter MJ, Nishioka NS, Kava LE, Rosenberg M, Bouma BE, Tearney GJ, Nat Med. 2013, 19, 238. [PubMed: 23314056]

[21]. Liang K, Traverso G, Lee HC, Ahsen OO, Wang Z, Potsaid B, Giacomelli M, Jayaraman V, Barman R, Cable A, Mashimo H, Langer R, Fujimoto JG, Biomed Opt Express. 2015, 6, 1146. [PubMed: 25909001]

[22]. Drexler W, Morgner U, Kartner FX, Pitris C, Boppart SA, Li XD, Ippen EP, Fujimoto JG, Opt Lett. 1999, 24, 1221. [PubMed: 18073990]

[23]. Tumlinson AR, Povazay B, Hariri LP, McNally J, Unterhuber A, Hermann B, Sattmann H, Drexler W, Barton JK, J Biomed Opt. 2006, 11, 064003. [PubMed: 17212526]

[24]. Wang DL, Hunter BV, Cobb MJ, Li XD, Ieee J Sel Top Quant. 2007, 13, 1596.

[25]. Xi JF, Zhang A, Liu Z, Liang WX, Lin LY, Yu S, Li XD, Opt Lett. 2014, 39, 2016. [PubMed: 24686663]

[26]. Yuan W, Mavadia-Shukla J, Xi JF, Liang WX, Yu X, Yu S, Li XD, Opt Lett. 2016, 41, 250. [PubMed: 26766686]

[27]. Mavadia-Shukla J, P. F WX, Liang S Wu C, Sears XD. Li. Biomed Opt Express. 2018, 9, 3731. [PubMed: 30338151]

[28]. Geary JM, Introduction to lens design: with practical ZEMAX examples Willmann-Bell, Inc, Richmond, 2002, pp.177.

[29]. Herz PR, Chen Y, Aguirre AD, Schneider K, Hsiung P, Fujimoto JG, Madden K, Schmitt J, Goodnow J, Petersen C, Opt Lett. 2004, 29, 2261. [PubMed: 15524374]

[30]. Li J, de Groot M, Helderman F, Mo J, Daniels JM, Grunberg K, Sutedja TG, de Boer JF, Opt Express. 2012, 20, 24132. [PubMed: 23187176]

[31]. Ahsen OO, Lee HC, Giacomelli MG, Wang Z, Liang K, Tsai TH, Potsaid B, Mashimo H, Fujimoto JG, Opt Lett. 2014, 39, 5973. [PubMed: 25361133]

[32]. Mavadia-Shukla J, Zhang J, Li KY, Li XD, Opt Lett. 2017 (in revision).

[33]. Chiu KW, Lu LS, Chiou SS, World J Exp Med. 2015, 5, 33. [PubMed: 25699232]

[34]. Suter MJ, Jillella PA, Vakoc BJ, Halpern EF, Mino-Kenudson M, Lauwers GY, Bouma BE, Nishioka NS, Tearney GJ, Gastrointest Endosc. 2010, 71, 346. [PubMed: 19879573]

[35]. Haggitt RC, Hum Pathol. 1994, 25, 982. [PubMed: 7927321]

[36]. Wang T, Pfeiffer T, Regar E, Wieser W, van Beusekom H, Lancee CT, Springeling G, Krabbendam I, van der Steen AF, Huber R, van Soest G, Biomed Opt Express. 2015, 6, 5021. [PubMed: 26713214]

[37]. van Soest G, Bosch JG, van der Steen AF, IEEE Trans Inf Technol Biomed. 2008, 12, 348. [PubMed: 18693502]

[38]. Uribe-Patarroyo N, Bouma BE, Opt Lett. 2015, 40, 5518. [PubMed: 26625040]

[39]. Salo JA, Salminen JT, Kiviluoto TA, Nemlander AT, Ramo OJ, Farkkila MA, Kivilaakso EO, Mattila SP, Ann Surg. 1998, 227, 40. [PubMed: 9445108]

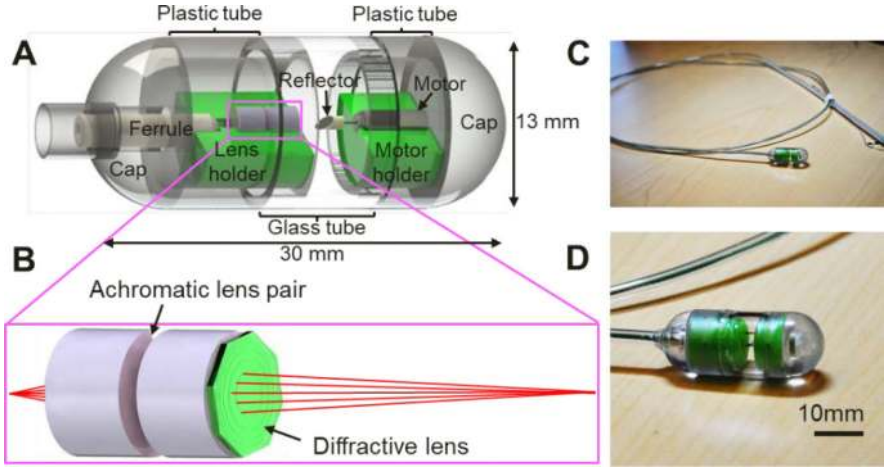

Figure 1.

Distal scanning tethered OCT imaging capsule operating at 800 nm. (**A**) Capsule design schematic consisting of a ferrule, achromatic optics, reflector, micromotor, holders and enclosure. (**B**) Schematic of the achromatic optics which includes two achromatic doublets lenses and one diffractive lens. (**C**) Photograph of the tethered capsule assembly. (**D**) Zoomed-in photograph of the capsule.

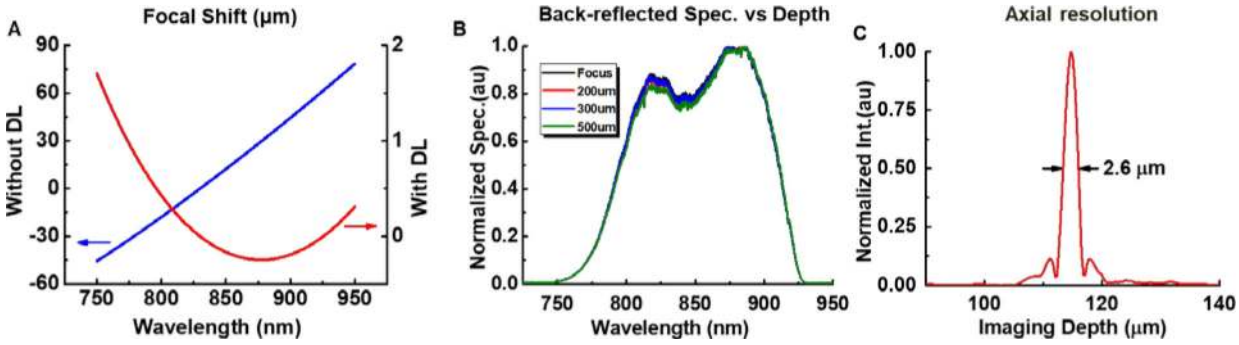

Figure 2.

Chromatic characteristics. (**A**) Longitudinal focal shift of two combined achromatic lenses over a full 200 nm bandwidth (blue curve), and the longitudinal focal shift after adding the diffractive lens to the two achromats (red curve). (**B**) Normalized spectra backscattered by a mirror placed at different positions along the imaging depth, which remained nearly unchanged, indicating the superb achromatic performance of the compound diffractive optics. (C) A representative axial point spread function from the capsule measured in air.

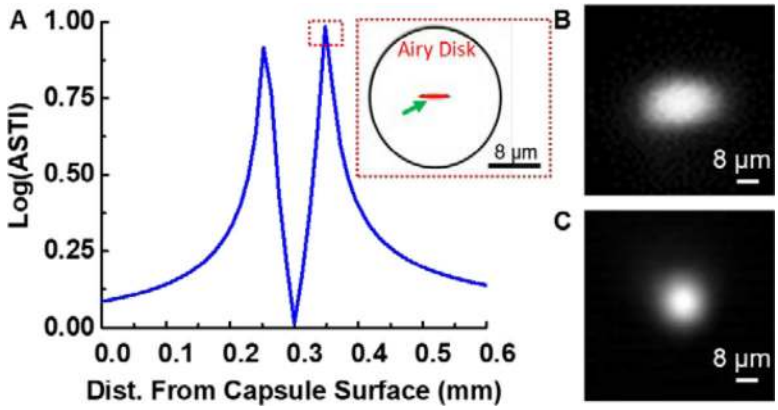

Figure 3.

Astigmatism performance within depth of field. (**A**) Logarithm of the ASTI defined as the ratio of the spot size in the azimuthal direction to that in the longitudinal direction. Inset: Airy disk and the worst spot shape indicated by a green arrow according to ZEMAX simulations. (**B**) The worst OCT imaging beam spot shape measured by a CCD camera within the DOF range which was about 50 μm away from the focal plane. (**C**) Imaging spot shape in the focal plane which was about 300 μm away from the capsule surface.

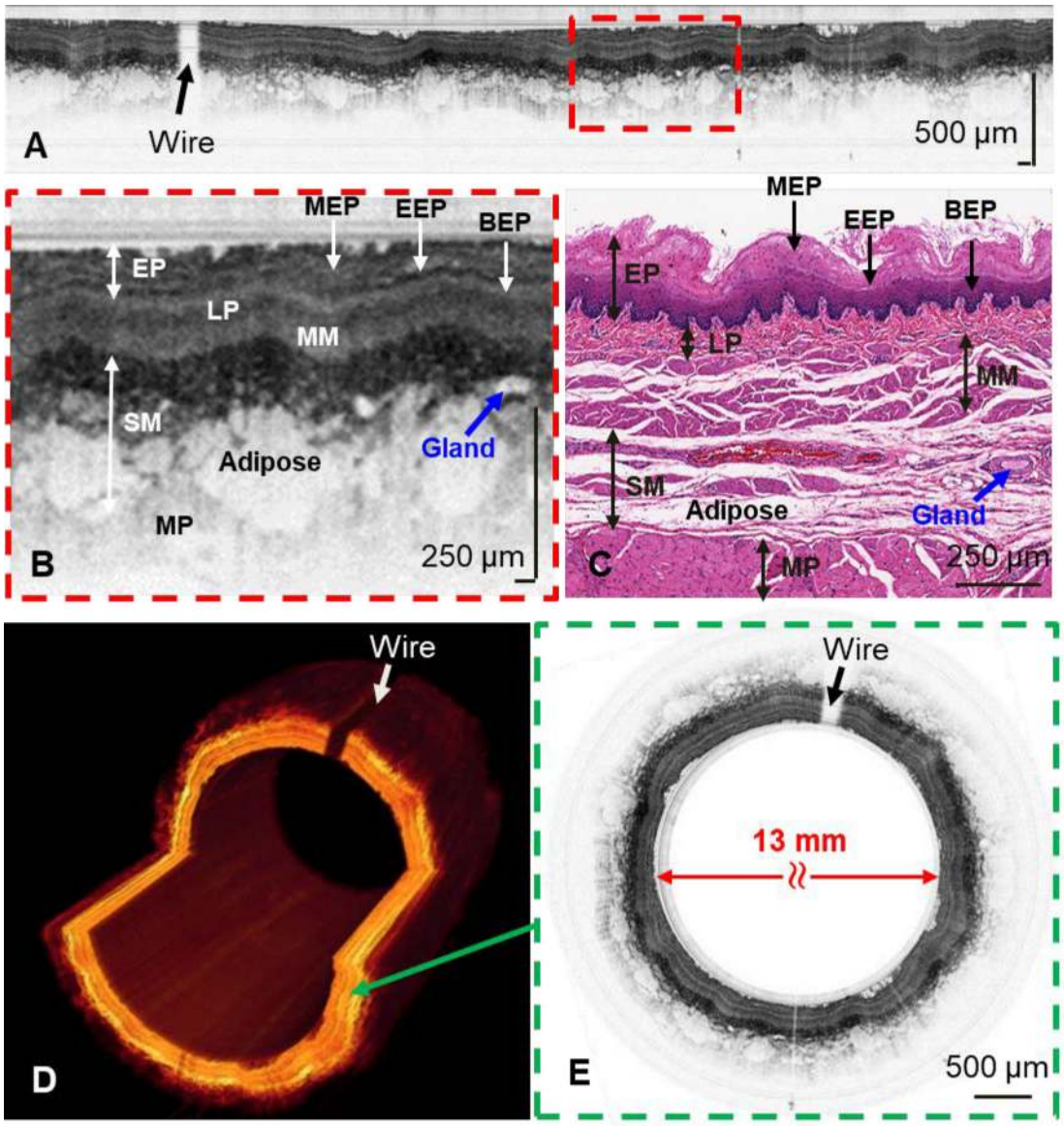

Figure 4.

Ex vivo imaging of swine esophagus. (**A**) Representative *ex vivo* flattened cross-sectional image of swine esophagus by the 800 nm OCT capsule (rectangular view). Fine micromotor wires (indicated by the arrow) block ~2% of the image. (**B**) Zoomed-in region corresponding to the red dashed box in **A**. Distinct layers can be clearly visualized: stratified squamous epithelium (EP) including mature epithelium (MEP), embryonic epithelium (EEP) and basal epithelium (BEP), lamina propria (LP), muscularis mucosae (MM), submucosa (SM), and muscularis propria (MP). (**C**) Representative swine esophagus histology micrograph. (**D**) 3D volumetric image of ~20 mm long lower swine esophagus. (**E**) The cross-section of the front surface pointed by the green arrow in **D**.

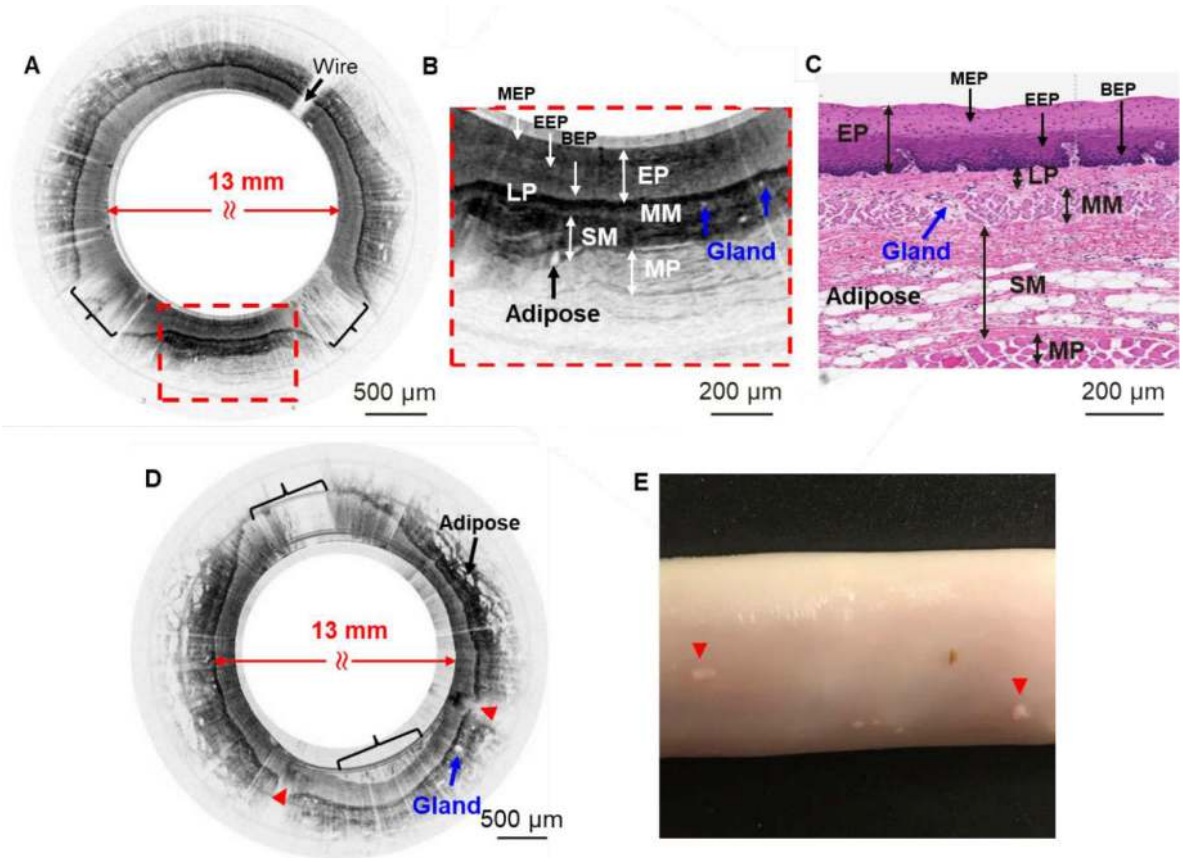

Figure 5.

In vivo imaging of sheep esophagus and laser ablation lesions. (**A**) A representative *in vivo* cross-sectional image of sheep esophagus before laser ablation. Two noncontact areas between the esophageal wall and the capsule were indicated by black brackets. (**B**) Zoomed-in region corresponding to the red dashed box in **A**, five layers can be visualized: EP including its sublayers MEP, EEP and BEP, LP, MM, SM, and MP. (**C**) A representative sheep esophagus H&E histology micrograph. (**D**) A representative *in vivo* cross-sectional image of sheep esophagus after laser ablation. Ablated areas are indicated by red arrowheads. The micromotor drive wires happened to be within the noncontact area indicated by black bracket at the 11 o'clock position. (**E**) A photo of laser ablated sheep esophageal tissue. The ablation spots are visible and indicated by red arrowheads.